Near-Field Scanning-Based Shielding Effectiveness Extraction for Board-Level Shielding Cans

Harsh Shrivastav , *Student Member, IEEE*, Takashi Enomoto, Shingo Seto, *Member, IEEE*, Kenji Araki, *Senior Member, IEEE*, and Chulsoon Hwang , *Senior Member, IEEE*

Abstract—The conventional definition of shielding effectiveness (SE) is well suited for calculations of far-field electromagnetic shielding. However, in the near field, SE calculations are not as straightforward. In radio-frequency interference (RFI) problems, the majority of field coupling occurs in the near field. Thus, a well-defined method for calculating the near-field SE is needed to estimate the suppression of RFI achieved by shielding cans. In this study, a method based on near-field scanning is developed to extract the SE of board-level shielding cans. The SE is defined by modeling the shielded noise source as equivalent dipole moments. The accuracy of the equivalent source is analyzed via the least-square error and correlation coefficient as confidence verification parameters. By applying the reciprocity theorem, the voltage coupled on a planar inverted F antenna from an unshielded and a shielded source is calculated. The coupled voltage from a shielded noise source serves as a reference to validate the effectiveness of the proposed method. Practical shielding cans were used to develop and validate the SE extraction method using full-wave 3D simulations and measurements.

Index Terms—Correlation coefficient, coupling, dipole moment, near-field scanning, planar inverted F antenna (PIFA), radio-frequency interference (RFI), reciprocity, shielding effectiveness (SE).

I. INTRODUCTION

ITH advancements in science and technology, modern electronic devices have become capable of establishing high-speed wireless connections. For example, a smartphone can wirelessly connect to a smart television, smart watch, smart home appliance, or smart audio speaker. Such connectivity is attributed to the presence of receiving/transmitting radio-frequency (RF) antennas. A typical smartphone has antennas for Wi-Fi, Bluetooth, a global positioning system (GPS), near-field communication (NFC), and various cellular bands. These RF antennas are located alongside high-speed digital clocks, processors, power management integrated circuits (ICs), and

Manuscript received July 26, 2019; revised December 17, 2019; accepted January 16, 2020. Date of publication February 25, 2021; date of current version August 13, 2021. This work was supported by the National Science Foundation under Grant IIP-1440110. (Corresponding author: Chulsoon Hwang.)

Harsh Shrivastav and Chulsoon Hwang are with the EMC Laboratory, Missouri University of Science and Technology, Rolla, MO 65401 USA (e-mail: hs5kb@mst.edu; hwangc@mst.edu).

Takashi Enomoto, Shingo Seto, and Kenji Araki are with the Sony Global Manufacturing and Operations Corporation, Tokyo 108-0075, Japan (e-mail: takshi.enomoto@sony.com; shingo.seto@sony.com; kenji.araki@sony.com).

Color versions of one or more figures in this article are available at https://doi.org/10.1109/TEMC.2021.3052815.

Digital Object Identifier 10.1109/TEMC.2021.3052815

differential data channels. If high-speed digital circuits are not properly designed and routed, they can easily couple to nearby RF antennas, causing radio receiver desensitization. To prevent RF interference (RFI) and desensitization problems, the use of well-designed shielding cans with accurately known shielding effectiveness (SE) values is important. General design rules, such as providing a good signal return path, locating potential noise sources away from large metal structures and reducing the length of transmission lines, have become increasingly difficult to meet with the growing demand for integration. Therefore, shielding enclosures are often employed to reduce interference from noise sources.

The SE of an enclosure is typically defined as the ratio of the incident field on the enclosure to the transmitted field through the enclosure. This definition is based on the assumption that the incident electromagnetic (EM) wave is a uniform plane wave with E and H fields in the far-field region. Radiated EM fields can be precisely measured by using an anechoic chamber. A measurement antenna can be placed in a chamber to measure the intensity of the EM field radiated by the shielded source and then contrasted with that measured by the antenna without the shield. The far-field SE can be efficiently and accurately calculated by using the conventional definition [1]; however, in the near field, the assumption that the EM wave behaves as a uniform plane wave is not valid. Furthermore, the impedance of the wave changes with the EM source type [2], which complicates calculations of the near-field SE. In RFI problems, the majority of field coupling occurs in the near field. Thus, a well-defined method for calculating the near-field SE is critical for quantifying the reduction in RFI achieved by shielding cans.

With ongoing research, multiple methods for defining and measuring the near-field SE have been developed. Gao *et al.* [3] defined the SE of system-in-package (SiP) modules based on the spatially averaged magnetic near field radiated from the SiP module. The SE definition was validated by correlating the far-field SE extracted using a reverberation chamber with the measured near-field SE. Kim *et al.* [4] proposed two new IC-stripline designs for measuring the near-field SE of on-board metallic cans, whereas Vanoost *et al.* [5] proposed a novel stripline design for characterizing the SE of board-level shielding cans in accordance with the stripline design described in standard SAE ARP 6248. Although in [3]–[5] methods for measuring the near-field SE are presented, the insight into the impact of the measured SE on the coupling between a shielded source and victim circuit is absent. Moreover, the shielding

0018-9375 \odot 2021 IEEE. Personal use is permitted, but republication/redistribution requires IEEE permission. See https://www.ieee.org/publications/rights/index.html for more information.

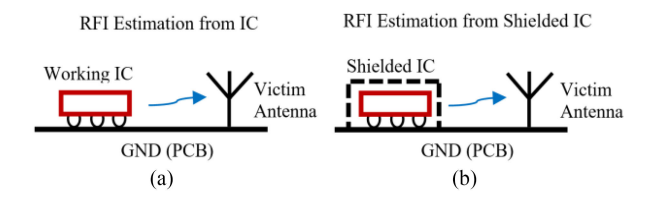


Fig. 1. RFI characterization from (a) an active IC and (b) a shielded IC.

cans analyzed in [3]–[4] were ideal, as they formed a complete Faraday cage around the source. Practical shielding cans have ventilation slots and castellated edges for thermal relief and reflow soldering. These slots and castellation gaps can act as antennas, thus changing the emission characteristics of the source beneath the shield [6]. Therefore, the radiation from slots on the shielding enclosure must be considered in extracting the SE. Hwang *et al.* [7] proposed an SE definition based on equivalent dipole moments, which were extracted using the transverse EM cell method. Although Hwang *et al.* [7] considered radiation from slots on the shielding can, this method is limited because the shielded source must be placed at the center of the evaluation board. For practical shielding cans, the equivalent dipole of the shielded source is not always located at the precise center, resulting in errors in the extracted SE values.

In this article, a new method for extracting the SE of board-level shielding cans using near-field scanning is proposed. The SE is defined by reconstructing the shielded source using equivalent dipole moments, which are extracted using near-field data from the shielded source. The use of near-field data enables a consideration of changes in source location and dipole type due to slots, castellations, and shielding can dimension. When multiple sources are present, near-field scanning can be used to focus on a specific shielded source and to obtain field data for the application of the proposed method. An analytical equation for estimating the voltage coupled on an RF antenna using the extracted SE is also formulated. Finally, the proposed method and formulations are validated through full-wave 3D simulations and measurements.

II. RFI SIMULATION WITH SHIELDED SOURCE

A typical RFI problem is illustrated in Fig. 1. Noise from an active IC and a shielded IC is coupled to an RF antenna in the near field, causing RFI. By analyzing the coupled voltage for the shielded source and the victim antenna, the suppression of RFI achieved by a shielding can was studied. All of the calculations were performed using full-wave simulations.

Using the multipole expansion theory [8], any arbitrary electrically small source can be modeled using a set of electric and magnetic dipole moments. The source is replaced with a set of appropriate electric dipoles P_x , P_y , and P_z and magnetic dipoles M_x , M_y , and M_z in Cartesian coordinates. As reported in [8]–[10], an active IC located above an infinitely large ground plane can be modeled using equivalent dipole moments (P_z , M_x , and M_y). Fig. 2 presents an active IC modeled with equivalent dipole moments. In general, the overall IC structure does not produce radiation. Instead, the radiation is dominated by a small portion of the IC, such as loops formed by wire bonds, which are

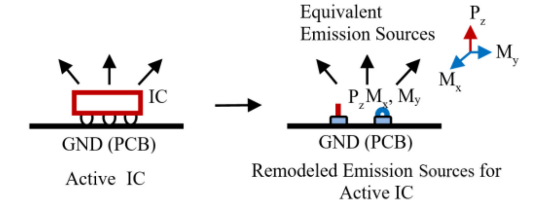


Fig. 2. Equivalent dipole moment model of an active IC.

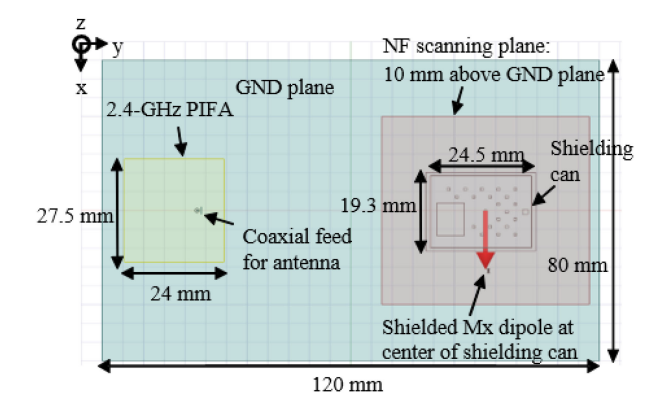


Fig. 3. Simulation model for estimating RFI and SE with a shielded ${\cal M}_x$ dipole source.

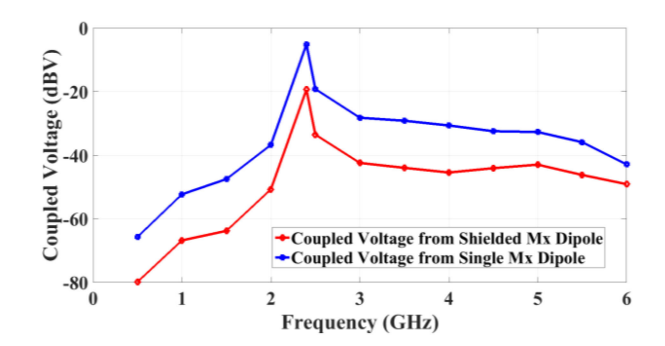


Fig. 4. Coupled voltage comparison between a single M_x dipole and a shielded M_x dipole.

electrically small for frequencies up to several GHz. Therefore, a magnetic dipole (current loop) can represent the emission from an IC reasonably well at the frequency of interest for RF communications. In this study, a magnetic dipole pointing in the x-direction (M_x dipole) is applied to approximate the noise from a working IC. The RFI is expressed as the voltage coupled from the source to the victim antenna, with the victim antenna terminated at 50 Ω . The EM field coupling from an M_x dipole and a shielded M_x dipole to a victim 2.4-GHz planar inverted F antenna (PIFA) was evaluated by designing a simulation model in ANSYS HFSS [11]. The strength of the M_x dipole is 1 Vm, and the simulation frequency range is 500 MHz-6 GHz. The simulation model applied to calculate the coupled voltage for the shielded M_x dipole is shown in Fig. 3. The voltage coupled to the PIFA can be calculated by integrating the E field along a tangential line connecting the signal and the signal return conductor on the coaxial feed of the antenna.

The coupled voltages on a PIFA due to a single M_x dipole and a shielded M_x dipole are shown in Fig. 4. The difference between the coupled voltage for a single M_x dipole and a

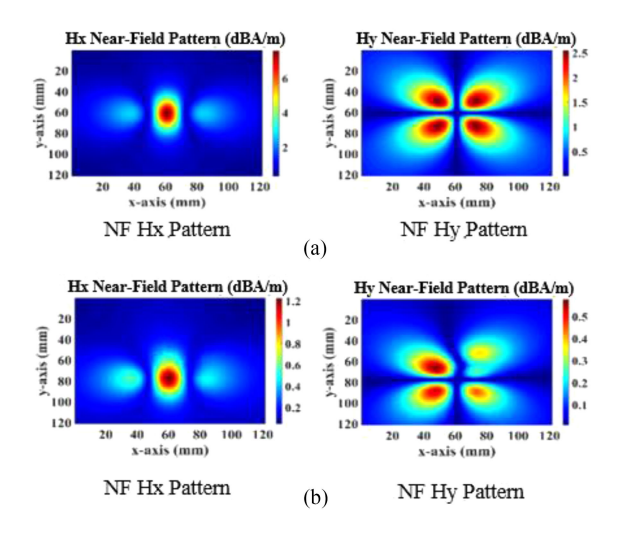


Fig. 5. Near-field patterns at a scan height of 10 mm from (a) a single M_x dipole and (b) a shielded M_x dipole.

shielded M_x dipole represents the RFI suppression achieved by the shielding can, i.e., the SE of the shielding can. In Section IV, the coupled voltage is estimated by using an analytical equation derived from the dipole-moment-based reciprocity method [12], [13]. Using the derived analytical equation, the proposed SE extraction method is then validated using 3D simulations and measurements.

III. NEAR-FIELD SCANNING-BASED SE EXTRACTION

A. SE Definition

Similar to an IC, a small shielding can enclosing an IC can also be modeled using equivalent dipole moments. Because the radiation primarily arises from a small portion of the shielding can (slots on the shield body), the source can be treated as electrically small, and the physics and equations presented in [7]–[10] can be applied to extract the equivalent dipole moments for the shielded source. Notably, RFI and desensitization issues that arise when the source behaves as a single dipole have been reported by numerous researchers [14]–[16]. Therefore, it is reasonable to assume that a single M_x dipole can represent an IC. With this assumption, a shielded M_x dipole can be modeled using equivalent dipole moments as follows.

Near-field patterns simulated above a single M_x dipole and a shielded M_x dipole at a frequency of 2.4 GHz and scan height of 10 mm are illustrated in Fig. 5. The design and geometrical details of the simulation model used to obtain the near-field pattern for the shielded M_x dipole are shown in Fig. 3. The strength of the M_x dipole is maintained at 1 Vm. As shown in Fig. 5, the near-field H_x and H_y patterns are approximately equivalent. The distortions in the shape of the near-field H_y pattern in Fig. 5(b) are due to the nonuniform slots on the shielding can body. Fig. 6 presents the geometrical details of the sheiding can. Due to the similarity in the shape of the near-field patterns, the shielding can enclosing the M_x dipole can be modeled in terms of equivalent dipole moments $(P_z', M_x', \text{ and } M_y')$. The workflow for modeling an active IC and a shielded IC with dipole moments is shown in Fig. 7.

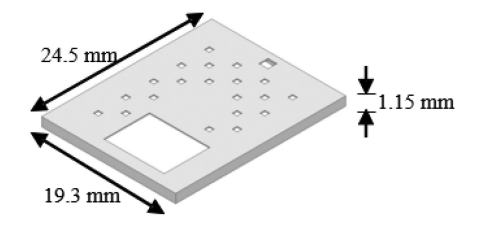


Fig. 6. Geometrical details of the structure used to shield the M_x dipole in Fig. 5(b).

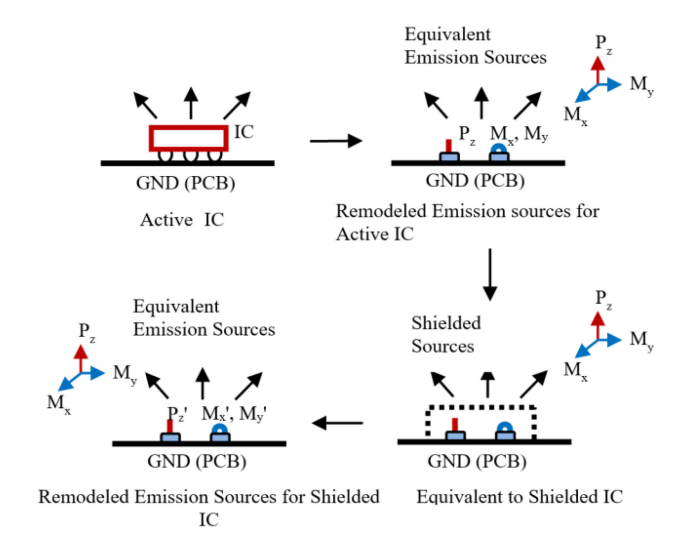


Fig. 7. Dipole moment representation of an active IC and shielded IC.

The combined effect of EM radiation from the source and slot antennas alters the radiation characteristics of the original source, causing an equivalent source transformation. Thus, a shielded M_x dipole may undergo an equivalent source transformation and act as an M_y dipole. Therefore, from an RFI viewpoint, the phenomenon of an equivalent source transformation must be considered when calculating the SE. An example of an equivalent source transformation is illustrated in Fig. 8. The H_x and H_y near-field patterns shown in Fig. 8 indicate that the shielded M_y dipole has undergone an equivalent source transformation and is now acting as a single M_x dipole instead of a single M_y dipole.

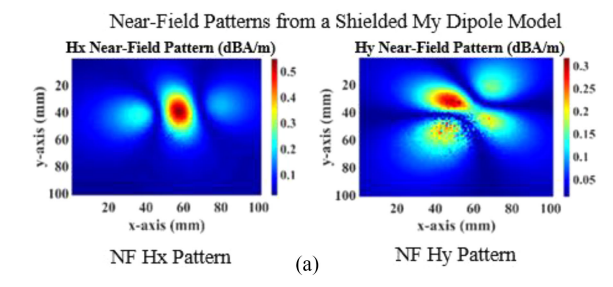
Equivalent dipole moments for a shielded source embody the physics of equivalent source transformations. Thus, using equivalent dipole moments, the SE is defined as follows [7]:

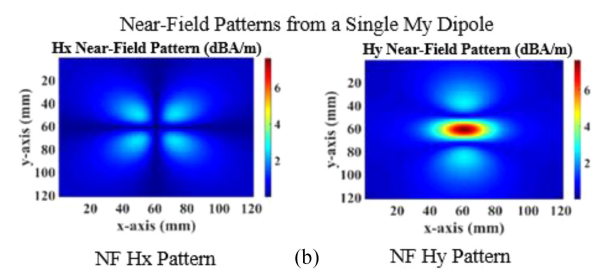
$$SE_{S_iS_j} = \frac{S_i}{S'_j} \tag{1}$$

where $S_i = P_z$, $k_0 M_x$, or $k_0 M_y$

$$S'_{i} = P'_{z}, k_{0}M'_{x}, \text{ or } k_{0}M'_{y}.$$

 S_i represents the magnitude of the dipole moments for an IC, whereas S_j' represents the magnitude of the equivalent dipole moments for a shielded IC. k_0 is the free space wave number, and the term k_0 has been introduced to render the SE unitless. The subscripted SE represents the SE value for the dipole component, which was created from the original dipole source via an equivalent source transformation. For example, SE_{PzMx}





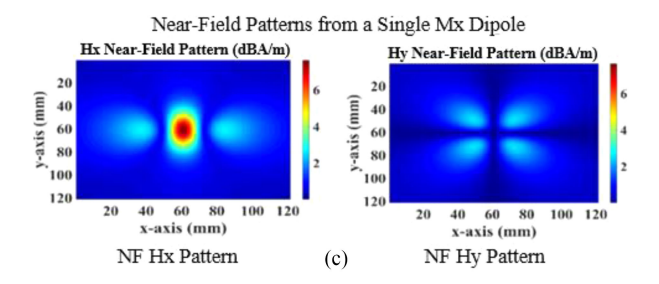


Fig. 8. Near-field pattern comparison for analyzing equivalent source transformations for (a) a shielded M_y dipole, (b) a single M_y dipole, and (c) a single M_x dipole.

represents the SE for an equivalent M_x dipole when a P_z dipole is the excitation source

$$SE_{PzMx} = |P_z| / |k_0 M_x'|$$
 (2)

The above SE definition will give the same results as a far-field-based SE measurement method if the considered source remains constant. Any change in the near field would be followed by an identical change in the far field. However, if an equivalent source transformation occurs, the far-field-based SE measurement method would fail to give an accurate SE, because it compares only ratios of the magnitude of the E or H field. Therefore, a near-field-based SE extraction method is required to capture the change in emission from the shielded source and to analyze its impact on RFI. With the source and shielded source modeled as dipole moments, the RFI for a dipole moment and victim antenna can be calculated by applying the reciprocity method [17]. Following the derivation in [18], the coupled voltage, $V_{\rm coupled}$, can be analytically calculated as

 $V_{\text{coupled}} =$

$$\frac{Z_L}{2V_{\text{rev}}^+} \left(-\overrightarrow{E}_{z,\text{rev}} \cdot \overrightarrow{P}_z + \overrightarrow{H}_{x,\text{rev}} \cdot \overrightarrow{M}_x + \overrightarrow{H}_{y,\text{rev}} \cdot \overrightarrow{M}_y \right) \tag{3}$$

where $H_{x,rev}$ and $H_{y,rev}$ are the x and y magnetic field components at the location of the dipole when the victim antenna

is excited, $E_{z, \mathrm{rev}}$ is the z component of the electric field at the dipole location in the reverse problem, P_z is the electric dipole moment in the z-direction, and M_x and M_y are magnetic dipole moments pointing in the x- and y-direction, respectively. Z_L represents a termination of 50 Ω for the victim antenna in the forward problem, and V_{rev}^+ represents the incident voltage excitation applied to the antenna in the reverse problem.

Depending on the dominant dipole moment representing the source, (3) can be simplified. For example, if an M_x dipole is used to represent the source, then the coupled voltage will be calculated as

$$V_{\text{coupled}} = \frac{Z_L}{2V_{\text{rev}}^+} \left(\overrightarrow{H}_{x,\text{rev}} \cdot \overrightarrow{M}_x \right).$$
 (4)

Using the SE definition proposed in (1), the voltage coupled to an antenna from a single M_x dipole (source) or shielded M_x dipole (shielded source) can be calculated as

$$|V_{\text{coupled},1}| = S_i \times TF \tag{5}$$

$$|V_{\text{coupled},2}| = S_i' \times TF \tag{6}$$

$$TF = \left| \frac{Z_L}{2V_{\text{rev}}^+} H_i \right| \tag{7}$$

where $V_{\rm coupled,1}$ represents the coupled voltage from a single M_x dipole and $V_{\rm coupled,2}$ represents the coupled voltage from a shielded M_x dipole. S_i is the dipole moment value of a single M_x dipole, S_j' represents the dipole moment value of an equivalent dipole representing the shielded M_x dipole, and H_i is the reverse H field measured at the location of the equivalent dipole moment. Then, $V_{\rm coupled,2}$ can be rewritten as

$$V_{\text{coupled},2} = \frac{S_i}{\text{SE}} \times TF.$$
 (8)

Using (8), the extracted SE obtained from the proposed method can be applied to estimate the voltage coupled on an antenna with a shielded source. Notably, the estimation applied in (8) is based on the assumption that no equivalent dipole transformation occurs.

B. Equivalent Dipole Moment Extraction

The dipole moments corresponding to an IC and a shielded IC must be accurately extracted to calculate the SE using (1). Assuming that an IC shielded by an enclosure can be modeled using equivalent dipole moments, the near-field scanning-based source reconstruction method is applied to extract the equivalent dipole moments. Here, tangential fields in the near-field scanning plane above the shielded source are used to calculate the equivalent dipole moments. Through source reconstruction based the measured H_x and H_y near-field patterns, any change in the radiation characteristics of the shielded source or in the location of the equivalent dipole moment can be taken into account. The tangential E and H fields measured in the near-field plane are related to the equivalent dipole moments by

$$F_n = T_{nk} X_k. (9)$$

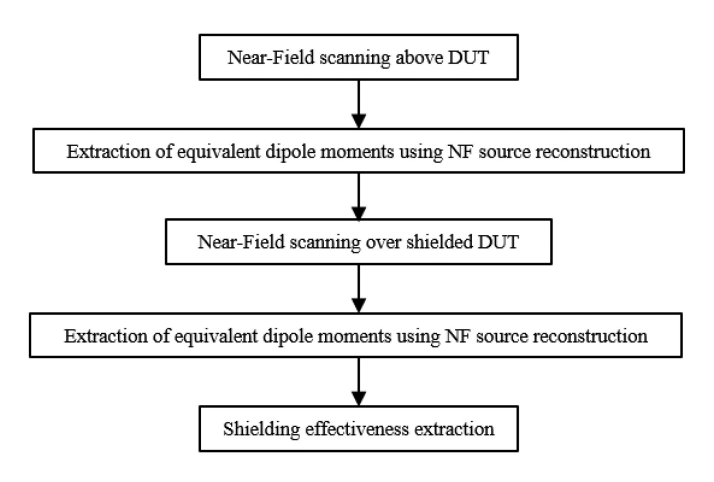


Fig. 9. Workflow for near-field scanning-based SE extraction.

An equivalent dipole moment matrix (X_k) is calculated by applying the linear least-square (LSQ) method

$$X_k = [T'_{nk} T_{nk}]^{-1} T'_{nk} F_n \tag{10}$$

where T'_{nk} represents the conjugate transpose of the T_{nk} matrix and F_n represents the tangential E and H fields [10].

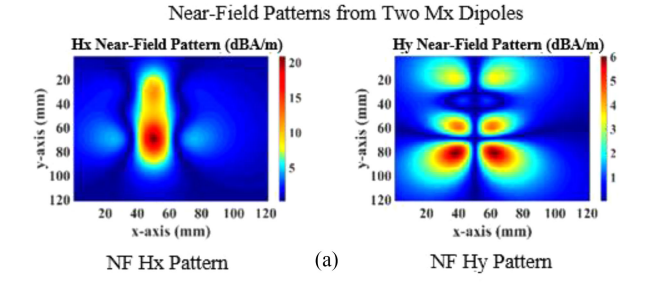
Using the calculated X_k values, the shielded source can be replaced by equivalent electric and magnetic dipole moments. The workflow for extracting the SE using near-field scanning is illustrated in Fig. 9.

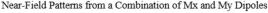
To implement the proposed SE extraction method, an assumption is made: The shielded source can be modeled using a single electric/magnetic dipole moment. For example, by applying the near-field source reconstruction method to the near-field patterns shown in Fig. 8(a), a shielded M_y dipole can be modeled using a single equivalent M_x dipole. The dipole moment of the equivalent M_x dipole will reflect the impact of geometry of the shielding can and the equivalent source transformation. However, depending on the emission properties of the source and the shielding can geometry, it may not be possible to model the shielded source with a single electric/magnetic dipole moment because the near-field patterns obtained from the source consist of more than one dipole (e.g., two M_x dipoles) or more than one type of dipole (e.g., one M_x dipole and one M_y dipole). Fig. 10 shows near-field patterns that differ from the near-field patterns of a single M_x dipole. To determine the accuracy with which a near-field pattern can be modeled using a single dipole moment, two confidence verification parameters are applied in this article: the LSQ error percentage [10] and the correlation coefficient (CC) [20].

Using these parameters, a near-field pattern can be distinguished if it can be reasonably approximated as a single dipole, which improves the confidence level of the near-field source reconstruction method of modeling a source using a single dipole moment. The LSQ percentage is defined as

$$\%Error = \frac{\left\| F_n - \hat{F}_n \right\|}{\|F_n\|} \times 100 \tag{11}$$

where F_n represents the E and H fields obtained from near-field scanning over the source and F_n represents the E and H fields





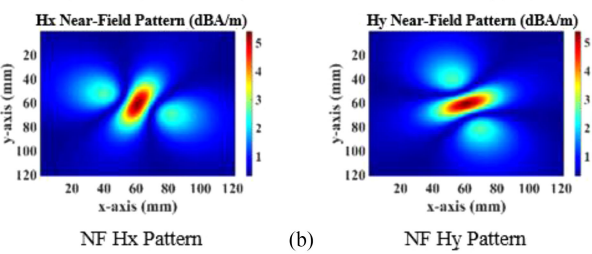


Fig. 10. Examples of near-field patterns in which the single dipole model assumption fails. (a) Near-field pattern from a source consisting of two M_x dipoles separated vertically. (b) Near-field patterns from a source consisting of one M_x dipole and one M_y dipole.

generated by the equivalent dipole moment of the source. The LSQ error percentage represents the fitting differences between fields measured by near-field scanning over the source and fields generated by the equivalent dipole source. A smaller LSQ error percentage corresponds to a better fit between the input and reconstructed near-field patterns and a more accurate calculation of the equivalent dipole moment.

The CC is defined as

$$r = \frac{\sum_{m} \sum_{n} (A_{mn} - \bar{A})(B_{mn} - \bar{B})}{\left(\sqrt{\sum_{m} \sum_{n} (A_{mn} - \bar{A})^{2} \cdot \left(\sum_{m} \sum_{m} (B_{mn} - \bar{B})^{2}\right)}\right)}$$
(12)

where \overline{A} represents the mean of A and \overline{B} represents the mean of B. m and n are the dimensions of datasets A and B. The shape vectors of the near-field pattern are applied to calculate the CC.

First, the contour function in MATLAB is applied to the near-field patterns to extract shape information from the pattern. Then, the RGB2Gray function is applied to the contour plot to obtain the values of the grayscale contour plot matrix, which reflects the significant shape contours (curvatures) of the near-field pattern, giving shape vectors. The CC for two near-field patterns quantitatively represents the similarity between the two patterns based on their shape. Patterns with a similar shape signature will have a CC close to 1.

To extract equivalent dipole moments using the near-field source reconstruction method, near-field patterns generated by a source are used as input. By examining a near-field pattern, one can assess the shape and intuitively guess whether the source can be modeled as a single electric/magnetic dipole moment. The LSQ error criterion quantifies this possibility with an appropriate value. A smaller LSQ error percentage implies that the source

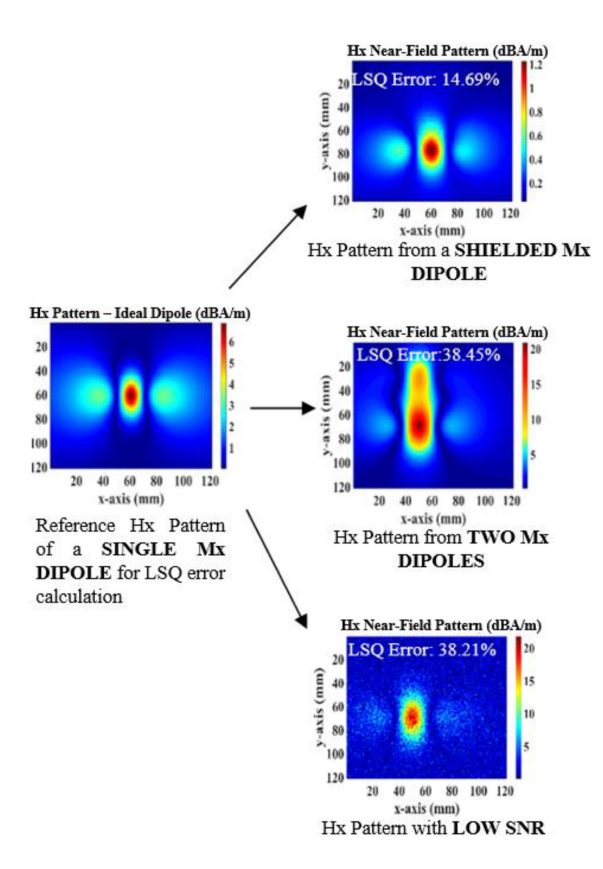


Fig. 11. Application of LSQ error for distinguishing near-field patterns.

can be modeled with great accuracy using a single type of dipole moment.

The application of the LSQ error is illustrated in Fig. 11, where H_x near-field patterns generated from a shielded M_x dipole, two M_x dipoles, and a pattern with a poor signal-to-noise ratio (SNR) are differentiated based on the LSQ error percentage. The H_x pattern from a single M_x dipole is used as a reference for calculating the LSQ error. The near-field pattern from a shielded M_x dipole gives an LSQ error of 14.69%, whereas the near-field pattern from two M_x dipoles gives an LSQ error of 38.45%, indicating that the shielded M_x dipole source can be more accurately modeled by a single equivalent M_x dipole moment than a source with two M_x dipoles.

In any type of measurement, the SNR is an important measurement parameter. A high SNR is always desirable and enables the measurement of weak signals. However, it is not always possible to obtain a high SNR. For near-field scanning, the SNR and number of points in the scan area determine the resolution of the measured near-field pattern. As shown in Fig. 11, the H_x pattern for a low SNR matches well with the reference H_x pattern. However, the LSQ error percentages for the H_x pattern for two M_x dipoles and the H_x pattern for a low SNR do not indicate which pattern is better suited for the near-field source reconstruction method. Using the CC, the H_x pattern for a low SNR dipoles can be differentiated from the H_x pattern for a low SNR based on the shape vectors. Fig. 12 illustrates the application of the CC to the aforementioned H_x near-field patterns. To calculate the CC, the near-field patterns shown in Fig. 11 are

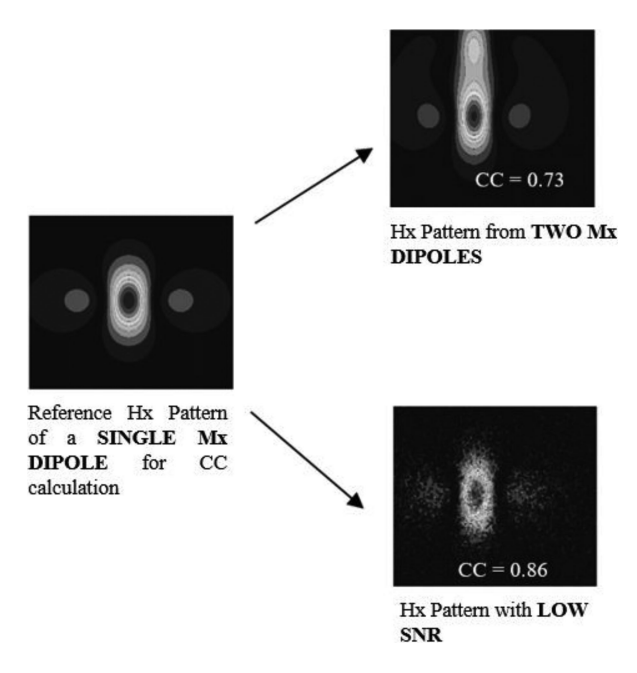


Fig. 12. Application of the CC for distinguishing near-field patterns.

represented by their shape vectors, which contain information about the contours/signature of the pattern. The CC represents the similarity between the shape of a near-field pattern and a reference pattern. For example, as shown in Fig. 12, the H_x pattern for two M_x dipoles has a CC of 0.73, whereas the H_x pattern with a low SNR has a CC of 0.86, indicating that, in terms of the shape of the near-field pattern, the H_x pattern with a low SNR matches the reference H_x pattern more closely. Thus, although the LSQ errors for the H_x pattern for two M_x dipoles and the H_x pattern with a low SNR are similar, the CC results indicate that the near-field pattern for a low SNR can be more accurately modeled by a single M_x dipole moment when using the near-field source reconstruction method. By comparing the LSQ error and CC of the near-field patterns, one can improve the confidence level of the near-field source reconstruction method in modeling a source using a single type of equivalent dipole moment. Near-field patterns generated by multiple dipoles can be modeled with a single type of dipole moment using a different approach.

As we move away from a multiple-dipole source, the multiple dipoles tend to converge into a single dipole, with the net dipole moment value determined by the phase relationship among the individual dipoles. The converged dipole moments retain the location of the dominant dipole among the multiple dipoles. By measuring near-field patterns for a height at which the dipoles converge, a source with multiple dipoles can be modeled as a single equivalent dipole. For example, Fig. 13 shows near-field patterns generated by a single M_x dipole and two M_x dipoles at a scan height of 10 mm. At this height, the near-field pattern from the source with multiple dipoles clearly shows the presence of two M_x dipoles. As the height of the near-field scanning plane increases, the patterns for the two M_x dipoles begin to converge into a single M_x dipole pattern. Fig. 14 shows near-field patterns generated from a single M_x dipole

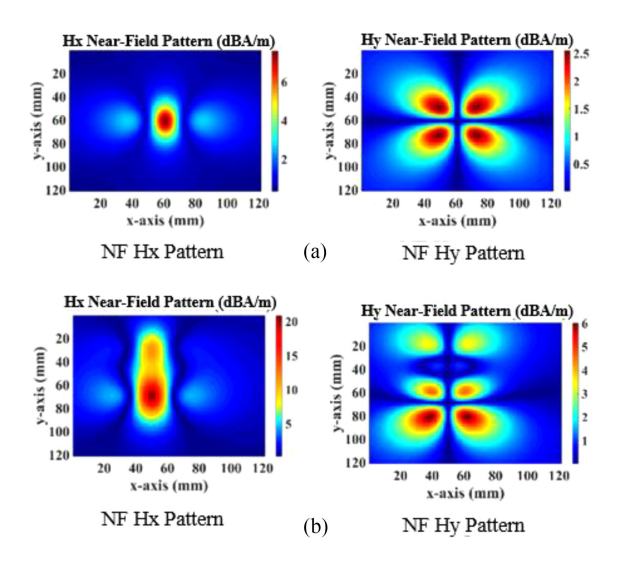


Fig. 13. Near-field pattern at a scan height of 10 mm for (a) a single M_x dipole and (b) two M_x dipoles.

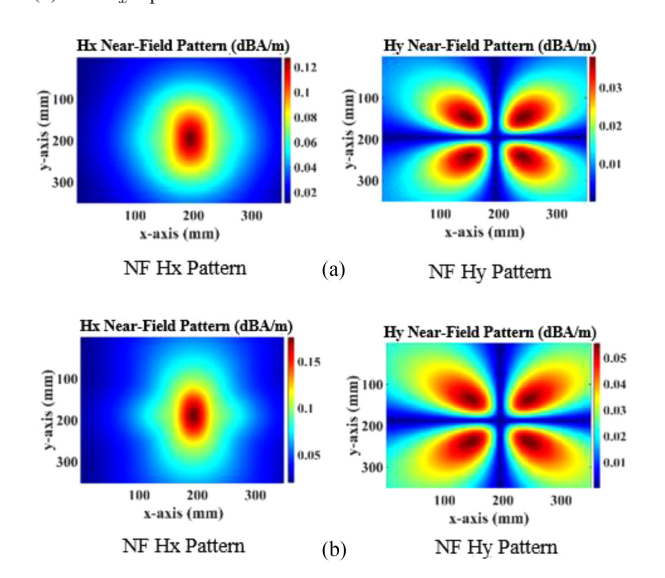


Fig. 14. Near-field pattern at a scan height of 65 mm for (a) a single M_x dipole and (b) two M_x dipoles.

TABLE I LSQ Error and CC for $H_{\rm x}$ Patterns for a Single $M_{\rm x}$ Dipole and Two $M_{\rm x}$ Dipoles at a Scan Height of 10 and 65 mm

	NF Scan Height: 10mm	NF Scan Height: 65mm
LSQ Error %	38.45	7.43
CC	0.73	0.94

and converged M_x dipoles at a scan height of 65 mm, which are approximately equivalent to each other. The accuracy with which two M_x dipoles source can be modeled by a single M_x dipole moment can be analyzed by calculating the LSQ error and CC. Table I presents the values of the confidence verification parameters calculated for the H_x near-field patterns illustrated in Figs. 13 and 14. At a scan height of 65 mm, the LSQ error is decreased by almost 80%, and the CC is very close to 1. This result demonstrates that by using the near-field patterns at a scan

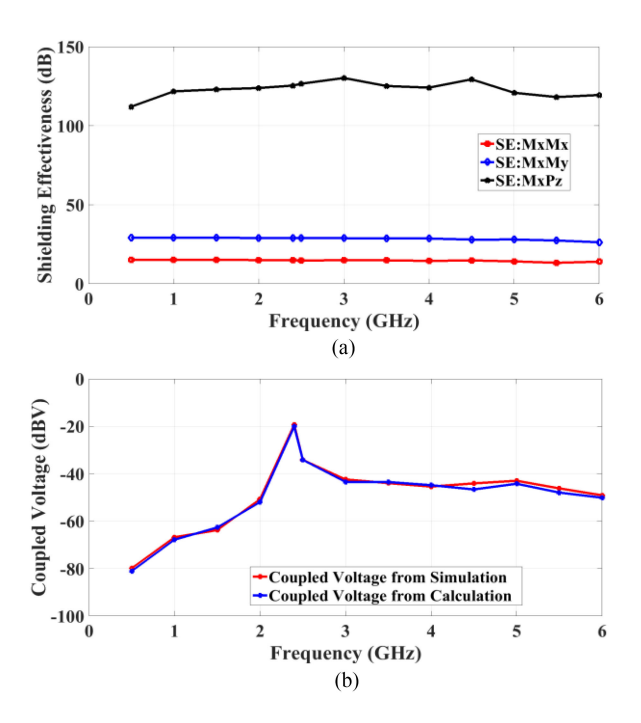


Fig 15. Extracted values for shielding can model A. (a) Extracted SE with M_x source excitation. (b) Coupled voltage validation with M_x source excitation.

height of 65 mm, one can model a source with two M_x dipoles as a single equivalent M_x dipole with high confidence by applying the near-field source reconstruction method. The single dipole representation for multiple dipoles allows one to extract the SE of a metallic can intended for simultaneously shielding two or more sources.

IV. VALIDATION OF EXTRACTED SE

A. Validation Using Full-Wave 3D Simulations

A magnetic dipole pointing in the x-direction (M_x dipole) representing an active IC is used as an excitation source for calculating the SE for two shielding can models: model A and model B. Both models are practical shielding cans used for suppressing RFI in the circuit board of a mobile device. The voltage coupled on a 2.4-GHz PIFA with a shielded source is estimated by performing simulations and applying the analytical equations discussed in Sections II and III. The correlation between the simulated and calculated coupled voltage is then used to validate the proposed SE extraction method.

The simulation model for calculating the coupled voltage and extracting the SE from shielding can model A is shown in Fig. 3. The strength of the excitation source, an M_x dipole, is 1 Vm, and the frequency range of interest is 500 MHz–6 GHz. Fig. 15(a) shows the variation in SE calculated using (1) for shield can model A over the frequency range of interest. Notably, the extracted value of SE_{MxMx} varies from 14–15.2 dB over the frequency range of interest. SE_{MxMy} and SE_{MxPz} , which represent SE values for the parasitic dipoles created from the shielded M_x dipole, are higher than SE_{MxMx} over the entire frequency range. The strength of a parasitic dipole is usually very low compared with that of the source M_x dipole. Therefore, the

TABLE II
LSQ ERROR AND CC VALUES CALCULATED FOR SHIELD CAN MODEL A WITH
$M_{ m x}$ Source Excitation

Frequency (GHz)	LSQ Error %	CC
0.5	14.68	0.89
1	14.29	0.86
1.5	14.94	0.89
2	14.48	0.88
2.4	11.12	0.87
2.5	13.79	0.88
3	13.51	0.89
3.5	13.49	0.85
4	11.45	0.84
4.5	19.48	0.78
5	14.12	0.83
5.5	18.88	0.80
6	15.21	0.84

extracted SE value for the parasitic dipoles is higher than that of the source dipole. The calculated SE will be accurate only if the equivalent single M_x dipole representing the shielded M_x source is extracted correctly using the near-field source reconstruction method. The confidence level of the equivalent dipole moment is analyzed by calculating the LSQ error and CC, as described in Section III. Table II shows the LSQ error and CC calculated using the equivalent single M_x dipole moment in the frequency range of 500 MHz-6 GHz. From this table, it is evident that the LSQ error is less than 20% at all frequencies, while the CC is close to 1, indicating that the equivalent single M_x dipole representing the shielded M_x source is accurately extracted by the near-field source reconstruction method. In other words, the extracted SE is correct. The threshold value for the confidence verification parameters can be set based on the tolerable error between the calculated and simulated coupled voltage for the shielded M_x dipole. The variation in the coupled voltage from the shielded M_x dipole over the frequency range of 500 MHz–6 GHz is shown in Fig. 15(b). The simulated coupled voltage is calculated as described in Section II, whereas the calculated coupled voltage is obtained by applying (8) with an equivalent single M_x dipole moment. The difference between the simulated and calculated coupled voltage is less than 1 dB.

The simulation model for estimating the coupled voltage and extracting the SE for shielding can model B is shown in Fig. 16, and the extracted SE curve and coupled voltage correlation are shown in Fig. 17(a) and (b), respectively. The extracted SE $_{MxMx}$ for shielding can model B varies from 10.8–15 dB over the frequency range of interest, and the SE values for the parasitic dipoles (SE $_{MxPz}$ and SE $_{MxMy}$) are higher than that for the source M_x dipole. The error between the simulated and calculated coupled voltage is less than 0.5 dB. The calculated coupled voltage was obtained by using (8) for an equivalent single M_x dipole moment. The calculated LSQ error was less than 15% over the majority of the frequency range, and the CC was higher than 0.90. For the LSQ error and CC calculations, only an equivalent single M_x dipole was used.

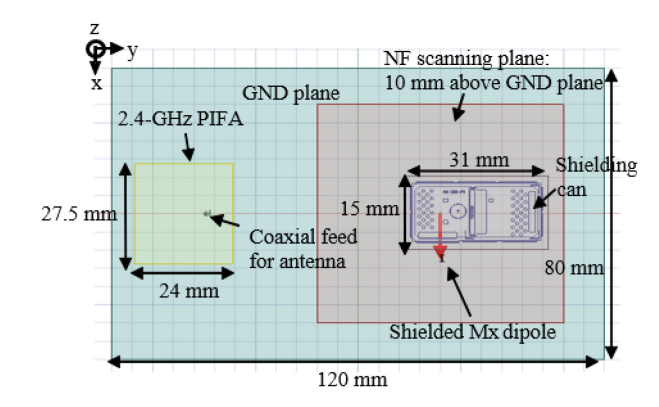


Fig. 16. Simulation model for estimating the RFI and SE of shielding can model B with M_x source excitation.

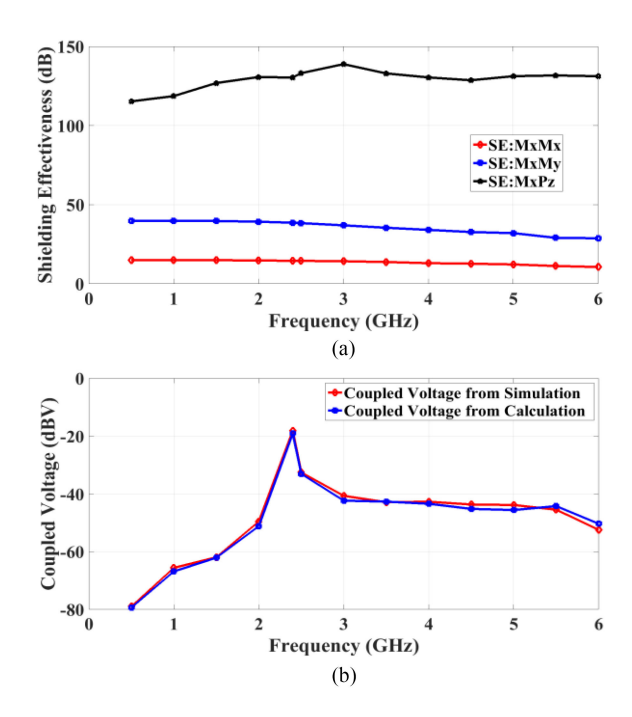


Fig 17. Extracted values for shielding can model B. (a) Extracted SE with M_x source excitation. (b) Coupled voltage validation with M_x source excitation.

The proposed SE extraction method was also applied in the case of an equivalent source transformation. The occurrence of an equivalent source transformation is dependent on the presence of slots, apertures, and castellated edges and the dimensions of the shielding can. The near-field patterns shown in Fig. 8(a) provide an example of an equivalent source transformation. These near-field patterns were generated by an M_y dipole source shielded by shielding can model A. The design and geometry of the simulation model used for calculating the coupled voltage and extracting the SE for the shielded M_{ν} dipole are the same as that in Fig. 3, with the exception that the excitation source is an M_y dipole instead of an M_x dipole. The strength of the M_y dipole is maintained at 1 Vm, and the simulation is performed over the frequency range of 500 MHz-6 GHz. Based on the near-field patterns shown in Fig. 8, the shielded M_{ν} dipole undergoes an equivalent source transformation and acts as an M_x dipole.

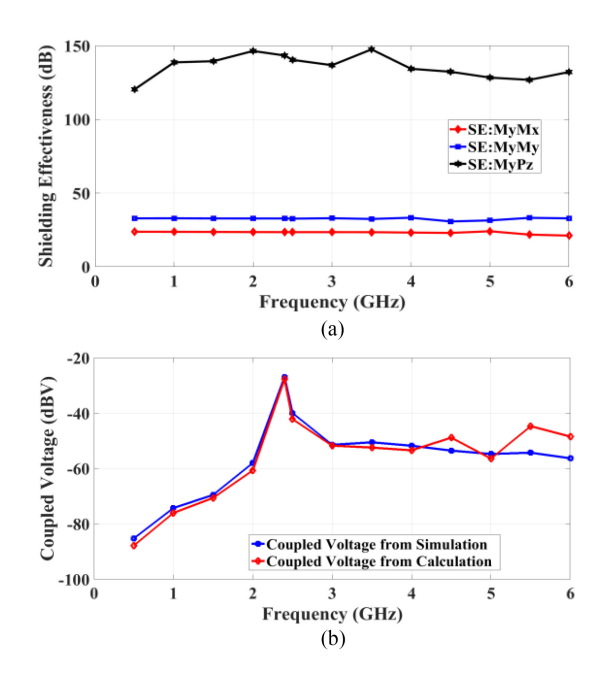


Fig 18. Extracted values for shielding can model A with equivalent source transformation. (a) Extracted SE with M_y source excitation. (b) Coupled voltage validation with M_y source excitation.

TABLE III LSQ Error and CC Values Calculated for Shield Can Model a With $M_{
m V}$ Source Excitation

Frequency (GHz)	LSQ Error %	CC
0.5	15.05	0.87
1	15.08	0.86
1.5	14.87	0.89
2	14.47	0.84
2.4	10.54	0.85
2.5	13.44	0.89
3	12.35	0.87
3.5	11.87	0.85
4	11.83	0.84
4.5	17.48	0.77
5	12.92	0.83
5.5	19.77	0.65
6	14.36	0.70

The SE extracted using (1) for shielding can model A with M_y source excitation is shown in Fig. 18(a). SE $_{MyMx}$ is approximately 24.5 dB in the frequency range of 500 MHz–6 GHz. The correlation between the calculated and simulated coupled voltage is shown in Fig. 18(b). The error is less than 1.5 dB at frequencies below 4 GHz. At 4.5 GHz, the error is approximately 3 dB, and at 5.5 and 6 GHz, there is an approximately 8-dB difference between the calculated and simulated coupled voltage. For frequencies at which the error is greater than 1.5 dB, the near-field pattern from the shielded M_y dipole no longer resembles that of a single M_x dipole, as indicated by a larger LSQ error and smaller CC. Table III shows the calculated values of the confidence verification parameters for the SE extracted in the equivalent source transformation scenario.

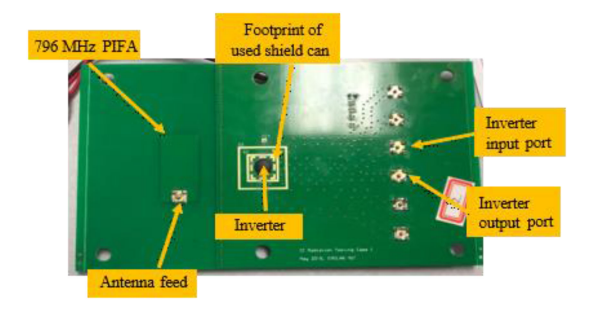


Fig. 19. Top view of the test board.

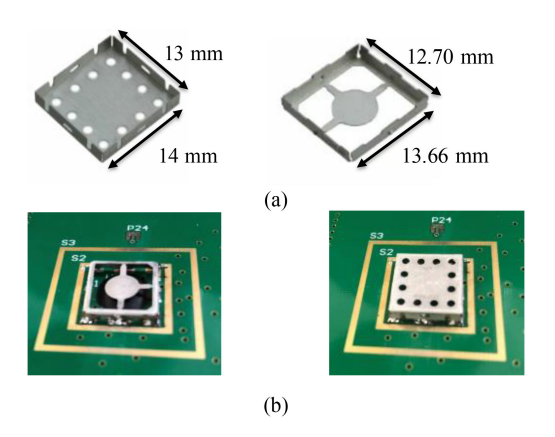


Fig. 20. Geometry and placement location of the two-piece shielding can. (a) Dimensions of the snap-fid lid and frame. (b) On board soldered shielding can.

B. Validation via Measurements

A test board was designed to validate the proposed SE extraction method using near-field and coupled voltage measurements. The test board primarily consists of an inverter die, a PIFA, and shielding can footprints. Fig. 19 shows the top view of the designed test board. The wire bondings of the inverter die were designed such that there is a current loop in the y-z plane, resulting in an M_x dipole. With this M_x dipole as source, the proposed method was applied to calculate the SE of a two-piece shielding can. Fig. 20 shows the geometrical details and on-board placement location of the shielding can. The measurements were performed at frequencies of 700–900 MHz in steps of 50 MHz.

To reconstruct the inverter and shielded inverter in terms of equivalent dipole moments, near-field scanning was performed over the test board, using an H-field probe with a loop size of 2 mm x 2 mm at a scan height of 7.7 mm. The H-field probe was calibrated using a 50- Ω microstrip trace to obtain the probe factor that includes the magnitude and phase information from the probe, amplifiers, and connecting cables. The size of the near-field scan plane was 40 mm x 40 mm, with a step size of 1 mm to obtain a high-resolution near-field pattern. The scan area and probe were positioned using an Amber Precision Instruments near-field scanner system. R&S FSV30 spectrum analyzer was used for scanning. Keeping the frequency of interest as the center frequency, a span of 1 kHz, an RBW setting of 50 Hz, and a positive peak detector with trace averaging, the noise floor of the spectrum analyzer was set sufficiently low to obtain a reasonable

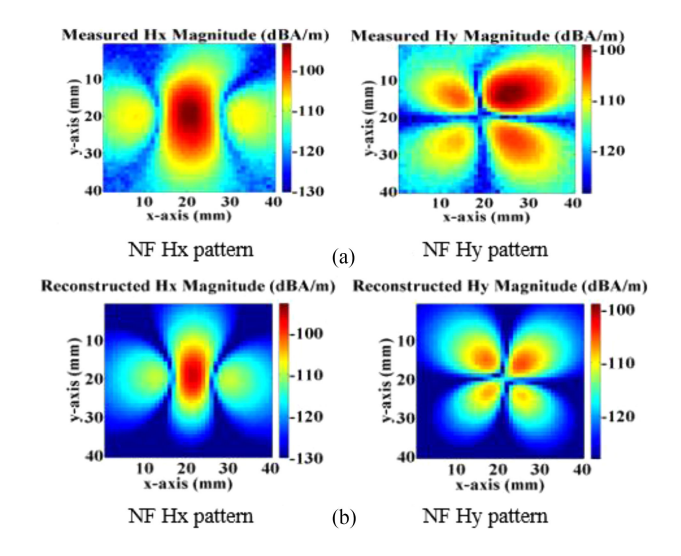


Fig. 21. Near-field pattern above a shielded inverter at a scan height of 7.7 mm. (a) Measured pattern. (b) Pattern obtained from the equivalent dipole moment of a shielded inverter.

SNR. The number of sweep points was 1601. The H-field probe was connected to the receiving end of the spectrum analyzer, and near-field measurements were performed in the allocated scan area to obtain the H_x and H_y near-field patterns over the inverter and shielded inverter. Using the measured data, near-field source reconstruction was performed to obtain the equivalent dipole moments. Fig. 21 shows the measured H_x and H_y near-field patterns over the shielded inverter and those generated by the equivalent dipole moment of the shielded inverter at 800 MHz. Because the SE is defined by the magnitude of the reconstructed dipole moments, phase information for the source M_x dipole is not required and was hence not acquired. Upon the extraction of equivalent dipole moments, the SE was calculated using (1).

To measure the voltage coupled to the PIFA, the shielded inverter, as shown in Fig. 20(b), was powered up, and the spectrum analyzer was connected to the antenna feed to measure the power coupled from the shielded inverter to the antenna. All of the near-field and coupled voltage measurements were performed in a shielded chamber to prevent any unintentional EM interference at the frequencies of interest. Using the extracted SE values, the coupled voltage was calculated using (8) and compared with the measured coupled voltage to verify the effectiveness of the proposed method. The extracted SE of the two-piece shielding can is displayed in Fig. 22(a). SE_{MxMx} varies from approximately 24 to 27 dB over the frequency range of interest. Because a parasitic dipole is weaker than the source M_x dipole, the SE value for the parasitic dipoles is higher than that for the source M_x dipole. The correlation between the measured and calculated coupled voltage for the shielded inverter is shown in Fig. 22(b). As expected, the maximum coupled voltage occurs at 800 MHz, which is close to the resonant frequency of the antenna (796 MHz). The difference between the measured and calculated coupled voltage is less than 2.2 dB. The discrepancy in the correlation is due to an insufficient SNR at 700, 750, and 900 MHz, even with the 50-Hz RBW setting in the spectrum analyzer. The LSQ error and CC shown in Table IV also indicate a discrepancy

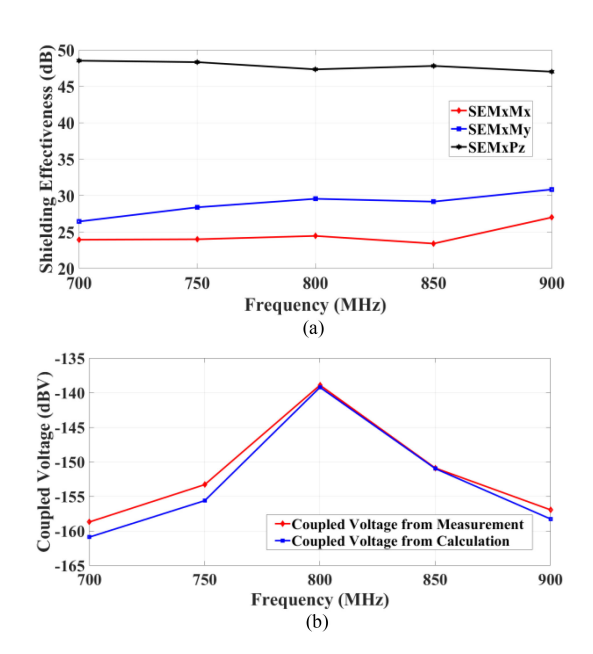


Fig. 22. Extracted values for a two-piece shielding can. (a) Extracted SE with M_x source excitation. (b) Coupled voltage validation with M_x source excitation.

TABLE IV LSQ Error and CC Values Calculated for a Two-Piece Shielding Can With $M_{\rm x}$ Source Excitation

Frequency (MHz)	LSQ Error %	CC
700	57.82	0.79
750	60.32	0.77
800	51.89	0.85
850	51.95	0.83
900	54.18	0.80

at these frequencies. It is worth mentioning that the tolerance level for LSQ error varies based on the acceptable discrepancy between measured and calculated coupled voltage. For example, if 50% LSQ error gave 0.5 dB difference between measured and calculated coupled voltage, then 50% LSQ error will be the acceptable tolerance level required to maintain 0.5 dB difference at all measurement frequencies. Agreement between measured and calculated coupled voltage will also reflect whether a single dipole model is adequate to represent the shielded source. Because the antenna exhibited the highest efficiency at 800 MHz, the agreement at this frequency is within 0.3 dB with LSQ error of 51.89%. Furthermore, multiple reflection may occur between the inverter and the body of shielding can, which can also cause differences in coupled voltage correlation.

V. CONCLUSION

A method for extracting the SE of a board-level shielding can using near-field scanning has been proposed in this work. The shielded source is modeled in terms of equivalent dipole moments using a near-field source reconstruction method. The SE is defined as the ratio of the dipole moment of the original source to that of the shielded source. The LSQ error and CC are applied to verify the confidence level of the equivalent dipole moment source reconstruction. Using the calculated SE, an

analytical equation is derived to estimate the coupled voltage on an embedded antenna due to a shielded source. The proposed method is validated by correlating the coupled voltages obtained from simulations, measurements, and the derived analytical equation. The phenomenon of equivalent source transformation due to the geometrical design of a shielding can is considered, and the SE is successfully extracted.

REFERENCES

- F. Vanhee, B. Vanhee, J. Catrysse, H. Yuhui, and A. Marvin, "Proposed methods to measure the shielding performance of PCB level enclosures," in *Proc. Int. Symp. Electromagn. Compat.*, Kyoto, Japan, 2009, pp. 689–692.
- [2] C. R. Paul, "Shielding," in *Introduction to Electromagnetic Compatibility*, 2nd ed. New York, NY, USA: Wiley, 2006, pp. 735–741.
- [3] L. Gao, X. C. Wei, Y. T. Huang, B. Li, and Y. F. Shu, "Analysis of near-field shielding effectiveness for the SiP module," *IEEE Trans. Electromagn. Compat.*, vol. 60, no. 1, pp. 288–291, Feb. 2018.
- [4] J. Kim and H. H. Park, "A novel IC-stripline design for near-field shielding measurement of on-board metallic cans," *IEEE Trans. Electromagn. Compat.*, vol. 59, no. 2, pp. 710–716, Apr. 2017.
- [5] D. Vanoost, T. Claeys, A. Degraeve, F. Vanhee, and D. Pissoort, "Dedicated stripline set-up for the characterization of the shielding effectiveness of board-level shields," in *Proc. Int. Symp. Electromagn. Compat.*, 2017, pp. 1–6.
- [6] C. A. Balanis, "Aperture antennas" in Antenna Theory Analysis and Design, 4th ed. New York, NY, USA: Wiley, 2016.
- [7] C. Hwang, J. D. Lim, G. Y. Cho, H. B. Park, and H. H. Park, "A novel shielding effectiveness matrix of small shielding cans based on equivalent dipole moments for radio-frequency interference analysis," *IEEE Trans. Electromagn. Compat.*, vol. 58, no. 3, pp. 766–775, Jun. 2016.
- [8] P. Wilson, "On correlating TEM cell and OATS emission measurements," *IEEE Trans. Electromagn. Compat.*, vol. 37, no. 1, pp. 1–16, Feb. 1995.
- [9] L. Li, J. Pan, C. Hwang, and J. Fan, "Radiation noise source modeling and application in near-field coupling estimation," *IEEE Trans. Electromagn. Compat.*, vol. 58, no. 4, pp. 1314–1321, Aug. 2016.
- [10] Z. Yu, J. A. Mix, S. Sajuyigbe, K. P. Slattery, and J. Fan, "An improved dipole-moment model based on near-field scanning for characterizing near-field coupling and far-field radiation from an IC," *IEEE Trans. Electromagn. Compat.*, vol. 55, no. 1, pp. 97–108, Feb. 2013.
- [11] Ansys HFSS, 2019. [Online]. Available: www.ansys.com
- [12] S. Lee *et al.*, "Analytical intra-system EMI model using dipole moments and reciprocity," in *Proc. Asia-Pacific Int. Symp. Electromagn. Compat.*, 2018, pp. 1169–1173.
- [13] Q. Huang, T. Enomoto, J. Maeshima, K. Araki, J. Fan, and C. Hwang, "Accurate and fast RFI prediction based on dipole moment sources and reciprocity," in *Proc. DesignCon*, Jan. 30–Feb. 1, 2018.
- [14] Q. Huang et al., "Desense prediction and mitigation from DDR noise source," in Proc. IEEE Int. Symp. Electromagn. Compat., Jul. 2018, pp. 139–144.
- [15] Q. Huang, F. Zhang, T. Enomoto, J. Maeshima, K. Araki and C. Hwang, "Physics-based dipole moment source reconstruction for RFI on a practical cellphone," in *IEEE Trans. Electromagn. Compat.*, vol. 59, no. 6, pp. 1693–1700, Dec. 2017.
- [16] Y. Sun, H. Lin, B. Tseng, D. Pommerenke, and C. Hwang, "Mechanism and validation of USB 3.0 connector caused radio frequency interference," *IEEE Trans. Electromagn. Compat.*, vol. 62, no. 4, pp. 1169–1178, Aug. 2020.
- [17] C. A. Balanis, "Electromagnetic theorems and principles" in Advanced Engineering Electromagnetics, 2nd ed. New York, NY, USA: Wiley, 2012.
- [18] Q. Huang, T. Enomoto, S. Seto, K. Araki, J. Fan, and C. Hwang, "A Transfer Function Based Calculation Method for Radio Frequency Interference," *IEEE Trans. Electromagn. Compat.*, vol. 61, no. 4, pp. 1280–1288, Aug. 2019.
- [19] S. Pan, J. Kim, S. Kim, J. Park, H. Oh, and J. Fan, "An equivalent three dipole model for IC radiated emissions based on TEM cell measurements," in *Proc. IEEE Int. Symp. Electromagn. Compat.*, Fort Lauderdale, FL, USA, 2010, pp. 652–656.
- [20] L. Sheugh and S. H. Alizadeh, "A note on Pearson correlation coefficient as a metric of similarity in recommender system," in *Proc. AI Robot.*, 2015, pp. 1–6.



Harsh Shrivastav (Student Member, IEEE) received the B.S. degree in electrical and electronics engineering from SRM University, Chennai, India, in 2015, and the M.S. degree in electrical engineering from the EMC Laboratory, Missouri University of Science & Technology, Rolla, MO, USA, in 2019.

He was a High-Frequency Electromagnetics Application Engineer with Ansys, Inc., San Jose, CA, USA,. His research interests include EMI/EMC simulation and measurements, signal/power integrity in high-speed digital systems, and radio-frequency interference.



Takashi Enomoto received the B.S. degree in electrical engineering from the Kyoto Institute of Technology, Kyoto, Japan, in 1989.

He was an Electrical Engineer with Sony Corporation, Tokyo, Japan, in 1989. He has been in charge of ANT/RF design of consumer products. His research interests include the development of EMC/RFI measurement and simulation techniques.



Shingo Seto (Member, IEEE) received the B.S. and M.S. degrees in electrical engineering from Keio University, Yokohama, Japan, in 2004 and 2006, respectively.

He was an Electrical Engineer with Sony Corporation, Tokyo, Japan, in 2006. His research interests include the development of EMC/RFI measurement and simulation techniques.



Kenji Araki (Senior Member, IEEE) received the B.S. and M.S. degrees from Hosei University, Koganei, Japan, in 1991 and 1993, respectively, and the Ph.D. degree from the University of Electro-Communications, Tokyo, Japan, in 2009, all in electrical engineering.

He was an Electrical Engineer with Sony Corporation, Tokyo, in 1993, and is currently a Deputy General Manager and Principal Engineer with Sony Global Manufacturing & Operations Corporation, Tokyo. His research interests include signal integrity

(SI), power integrity (PI), electromagnetic interference (EMI), electrostatic discharge (ESD), radio frequency interference (RFI), and simulation for electromagnetic compatibility (EMC).

Dr. Araki is a senior member of the Institute of Electronics, Information, and Communication Engineers of Japan.



Chulsoon Hwang (Senior Member, IEEE) received the B.S., M.S., and Ph.D. degrees in electrical engineering from the Korea Advanced Institute of Science and Technology (KAIST), Daejeon, South Korea, in 2007, 2009, and 2012, respectively.

From 2012 to 2015, he was a Senior Engineer with the Global Technology Center, Samsung Electronics, Suwon, South Korea, where he was mainly engaged in radio-frequency interference design for mobile phones. In July 2015, he joined the Missouri University of Science and Technology (formerly Uni-

versity of Missouri-Rolla), Rolla, MO, USA, and is currently an Assistant Professor with the Missouri S&T EMC Laboratory, Rolla. His research interests include signal/power integrity in high-speed digital systems, inter/intra EMC, and three-dimensional IC integrations.